Document Number**:** H2020-ICT-52/RISE-6G/D7.3

Project Name:

Reconfigurable **I**ntelligent **S**ustainable **E**nvironments for **6G** Wireless Networks (RISE-6G)

Deliverable D7.3

Final results of Proof-of-Concepts & trials

Date of delivery:	30/12/2023	Version:	1.1
Start date of Project:	01/01/2021	Duration:	36 months

Deliverable D7.3

Final results of Proof-of-Concepts & trials

Project Number:	101017011
Project Name:	**R**econfigurable **I**ntelligent **S**ustainable **E**nvironments for **6G** Wireless Networks

Document Number:	H2020-ICT-52/RISE-6G/D7.3
Document Title:	Final results of Proof-of-Concepts & trials
Editor(s):	ORA (Dinh-Thuy Phan Huy)
Authors:	GNW (A. Shokair, A. Toubal, Y. Nasser), ORA (G. Grao, P. Ratajczak, D.-T. Phan Huy, C. Gallard, M.-H. Hamon), TIM (M. Crozzoli, E. Zimaglia, A. Allasia, D. Disco), CRF (D. Masera), SNCF (G. Morall Adell, M. Simon S. Ros), NEC (V. Sciancalepore, P. Mursia), CHA (S. He Zhongxia, H. Wymeersch), CEA (B. Denis, E. C. Strinati), CNIT (L. Bastianelli, V. Mariani Primiani).
Dissemination Level:	PU
Contractual Date of Delivery:	30/12/2023
Security:	Public
Status:	Final
Version:	1.1
File Name:	RISE-6G_WP7_D7.3_VF.docx

Abstract

In this deliverable, we have presented the final results on RIS field-trials with RIS prototypes developed by partners of the project.

A first trial has shown in Rennes SNCF Train station, that even without the Orange commercial 5G network and 5G smartphones (in the mmWave band) being aware of the RIS, the RIS could already bring a significant **gain of around 20 dB in RSRP**. This boosting could potentially also be converted into EMFEU boosting. In a second trial in a factory environment at CRF premises, RIS-based localisation was successfully validated on-field with commercial 5G equipment (in the mmWave band) operated by TIM. During the experiments it was observed that, due to RIS optimization, a signal level improvement **up to 20 dB**, under poor coverage conditions (NLoS) could be achieved. Other trials at 60 GHz and 140 GHz have tested RIS-aided localisation successfully. Also, based on the study of two prototypes (among which, one working with a battery during trials), it is likely that **future RIS prototypes will be able to operate with an order of magnitude less power than an active relay**. Additionally, a very preliminary experiment has shown that RIS can also be used to perform interference nulling and boost secrecy.

In **conclusion**, the project trials, some with RISE-6G RIS prototypes, commercial mobile network equipments and smartphones, show that RIS is a promising technology to boost connectivity and enable localization, achieving **up to 20 dB gain** of receive signal strength improvement. Regarding **outlooks**, **further steps are needed in the direction of implementation and standardisation**. Indeed, in current trials, a lot of radio optimization is performed offline and in a static manner. Innovations and techniques created in WP4, WP5 and WP6, that dynamically and jointly optimize BS transmission/reception, RIS tuning and exploiting smartphone feedbacks, will be necessary to provide a **fully operative and usable RIS-empowered networks**. Finally, more efforts are needed to produce more low-power RIS prototypes with a an order of magnitude less operating power than active relay.

Keywords

Beyond-5G; 6G; RIS; Scenarios; Proof-of-concept, Field Trials, Commercial Base Stations, Commercial devices, communication, localisation, electromagnetic field aware, secrecy.

Contents

List of Figures

List of Acronyms

2D	two dimensional
3D	three dimensional
3GPP	3rd generation partnership project
5G-NR	5th Generation - New Radio
64QAM	64 Quadrature Amplitude Modulation
ADB	Android Debug Bridge
AGV	Autonomous Guided Vehicle
ARCEP	Autorité de régulation des communications électroniques, des postes et de la distribution de la presse
BS	Base Station
CEA	Commissariat à l'énergie atomique
CHA	University of Technology of Chalmers
CNIT	Consorzio Nazionale Interuniversitario per le Telecomunicazioni
CPE	Customer Premises Equipment
CRF	Centro Ricerche Fiat
CSI	Channel State Information
DAC	digital analog converter
DL	Downlink
DL-DoD	Downlink Direction of Departure
DL-TDoA	Downlink Time Difference of Arrival
DoA	Direction of Arrival
DoD	Direction of Departure
EM	Electromagnetic
EMFE	electromagnetic field exposure
GNW	Greenerwave
KPI	Key-Performance Indicator
LoS	Line-of-Sight
MIMO	Multiple Inputs Multiple Outputs
MMIC	monolithic microwave integrated circuit
mmWave	millimeter wave
NLOS	non line of sight
OFDM	Orthogonal Frequency Division Multiplexing
ORA	Orange
OS	Operating System
RCS	radar cross section
RF	Radio Frequency
RIS	Reconfigurable Intelligent Surface
R-RIS	Reflective RIS

RSRP	Reference Signal Received Power
RX	Receiver
S-EMFEU	self-electromagnetic field exposure utility
SINR	Signal to Interference plus Noise Ratio
SNCF	Société nationale des chemins de fer français
SNR	Signal to Noise Ratio
TIM	Telecom Italia Mobile
TX	Transmitter
UE	User Equipment
UL	Uplink

1 Introduction

The RISE-6G project focuses on the ground-breaking technology, namely Reconfigurable Intelligent Surfaces (RIS), which is expected to play a major role in the rollout of the 6th generation (6G) of wireless and mobile networks. In particular, one of the important objectives of RISE-6G is to provide concrete means to demonstrate the feasibility of the proposed technology within different relevant scenarios by designing, building and integrating RIS prototypes and proof-of-concepts (PoCs).

This main objective is fully covered by the work-package 7 (WP7) that analyses and designs an overall RIS-aided network. Specifically, this has been obtained by assembling and integrating RIS prototypes and using commercial network equipments and commercial smartphones. RIS prototypes have been installed and tested in two main different field-trials that account for distinct environmental scenarios. The two setup demonstrates deployments scenarios identified in [D2.4]. The former setup has been installed in a real train station from Société nationale des chemins de fer français (SNCF), at Rennes, in France where Orange operates with its own 4G and 5G infrastructure. The latter has been installed in the premises of Centro Ricerche Fiat (CRF), a car-OEM, in a real industrial environment, where Telecom Italia Mobile (TIM) operates its own 5G infrastructure. In the first setup, RIS has been used to boost coverage. The same experiment also enables to confirm whether self-electromagnetic field exposure utility (S-EMFEU) as defined in [D2.4] can be boosted. In the second set-up, localisation with a single base station (BS) and in a factory environment has been enabled. Note that these setups validate deployment scenarios for coverage boosting, EMFEU boosting, localisation boosting, identified in [D2.3].

This deliverable follows up the previous published [D7.1] and [D7.2] and is organised as follows:

- Section 2 reports the results of the trial aiming at boosting Orange commercial 5G network coverage in SNCF Train Station thanks to RIS; it also explains how EMFEU could potentially be boosted with the same setup;
- Section 3 reports the trial aiming at enabling a RIS-based localisation procedure in CRF factory with TIM commercial 5G network equipment;
- Section 4 reports results on PoCs of RIS-aided localisation in other frequencies;
- Section 5 analyses the expected energy consumption and sustainability of RIS, based on RIS prototypes.
- Section 6 concludes this deliverable and provides outlooks.

In the annex, a preliminary experiment for secrecy boosting use case identified in [D2.3] is also reported. This experiment is an addition to the initially planned experiments.

2 Boosting the connectivity of a commercial 5G network at mmWave in a train station thanks to RIS

2.1 Setup

The trial took place inside SNCF Rennes Train Station in France [RS]. Experiments have been conducted at the 2nd floor, where travelers' access to the trains' platforms, help desks, ticket sales points, stores, and restaurants. The tests lasted for three days, therefore, under time varying propagation conditions, time-varying traffic, and time-varying crowd sizes.

The Orange network deployed in SCNF Train Station uses commercial 5G network equipments. The base station was a NOKIA base station installed on a beam near the ceiling at 5.9 meters height. The BS was transmitting at 24 dBm and using spectrum from 26.5 to 27.5 GHz. The total bandwidth was 800 MHz (thanks to aggregation of 100MHz bands) for the downlink (DL) and 200 MHz for the uplink (UL). The maximum EIRP is 60 dBm. The authorisation to use the spectrum (not yet allocated to 5G) for experiments has been provided by the French Regulator Autorité de régulation des communications électroniques, des postes et de la distribution de la presse (ARCEP). The network was a non-standalone 5G network, using a 4th generation (4G) Long Term Evolution (LTE) anchor band at 2100 MHz. Modulations schemes up to 64 QAM were supported. The 5G network could be configured through a computer. On the device side, several 5G traceable-smartphone devices were available, with radio log, under Android Operating System (OS). A SONY Xperia Pro supporting band n257 ([26.5-29.5] GHz), working in non-standalone mode, and supporting the aggregation of 8 CCs in DL and 2 CCs in UL, has been used for performance assessment.

The mmWave RIS has been provided by Greenerwave, with a computer equipped with software to control the RIS. Its bandwidth of operation was compatible with the spectrum of the 5G network. Before using any smartphone, Greenerwave has used a spectrum analyzer to check the received 5G signal at a given location. As no power plug was available close to the deployment location of the RIS, the RIS powered itself on a battery during all the trial. Note that Greenerwave RISes have been characterised in detail and tested in lab and in indoor with controlled sources, by WP3, in preparation of this trial, in [D3.1] [D3.2] [D3.4].

Note that the RIS used during the trial was battery powered during the trial. The RIS consumes 2 watts, 18 watts and 35 watts, in idle mode, average and at maximum, respectively. However, new prototypes with ten times lower energy consumption are being built.

Parameter	Value
Polarization	dual, Horizontal polarization and Vertical polarization
Half power beam width	3-5 degree (controllable)
Scan Range (Azimuth, Elevation)	+/-60 deg.
RF Power Handling	max 50W

Beamforming capabilities	Variable beamwidth. Multi-beaming
Power Consumption (idle, average, max)	2 W, 18 W, 35 W Battery-powered during the trial.
Active area size	200 mm x 200 mm

Table 2-1: Greenerwave RIS characteristics

2.2 Objective, use case and methodology

The objectives were to validate the operation and identify KPIs of the RIS in the targeted frequency range in a real environment using an operational 5G Frequency Range 2 (FR2) (i.e. mmWave) network. The tested use case was the following: to use the RIS to cover a poorly covered area with 5G mmWave, using narrow reflected beams with high gain to improve the received power and the achieved throughput. This experiment validates the feasibility of WP4 objectives in terms of connectivity boosting. It also indirectly validates the objectives of WP6 in terms of energy-efficiency and self-electromagnetic field exposure boosting. Indeed, boosting the link budget between the transmitter and the receiver can be either translated into connectivity boosting (for same amount of spent energy), energy-efficiency boosting or EMFE reduction (for same target quality of service).

As the 5G network is not aware of the RIS presence nor influence, the following two-step approach has been used:

- During step 1: as illustrated in Figure 2-1. Step 1 The RIS is configured using the method explained in [D3.4], which mixes a geometrical approach. If necessary, some additional fine-tuning based on feedback from the spectrum analyzer is possible.
- During step 2: the emulated device from step 1 is replaced by the traceable smartphone device downloading data over the 5G network, and the 5G data connection quality is assessed.

During none of these steps, the 5G BS mmWave **has never been aware of the RIS**. The 5G BS has been performing its dynamic beamforming as usual, based on the traceable smartphone device standardized 5G feedback (Rank Indicators, Channel State Information, Precoding Matrix Indicator etc.) without any change. It simply **operated in a propagation environment that had been improved by the RIS**.

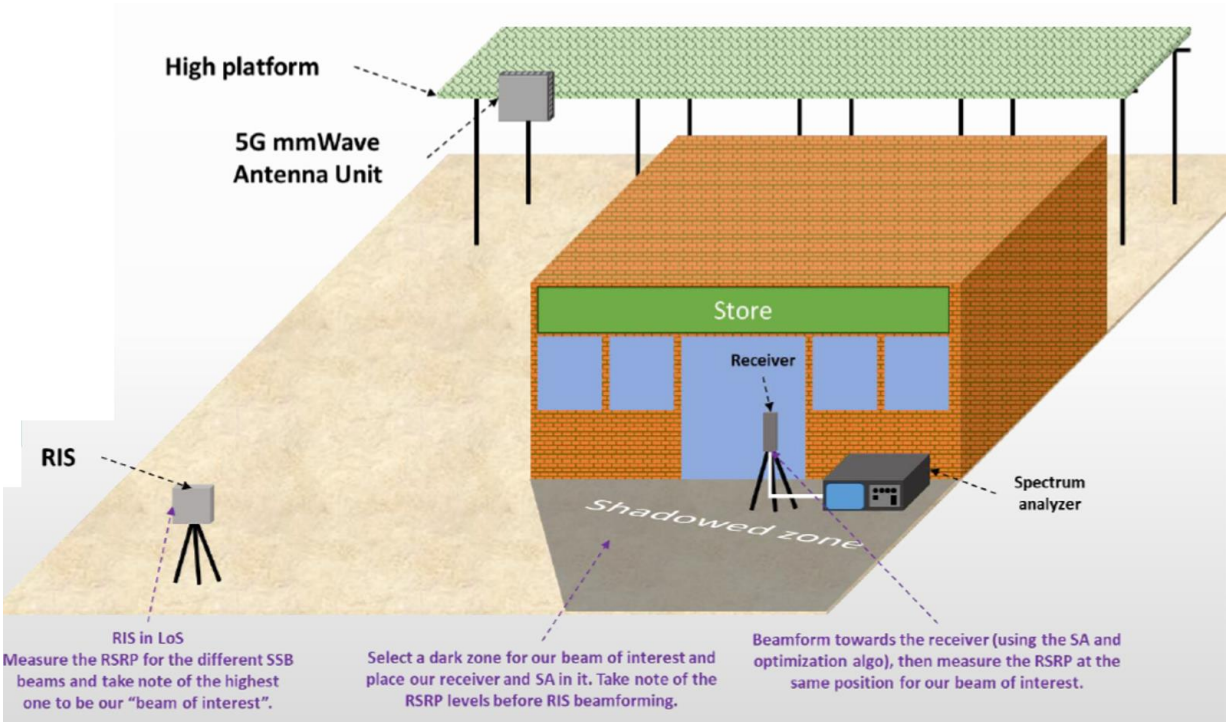

Figure 2-1. Step 1 setup, with the emulated device, i.e. the antenna and spectrum analyzer (SA).

Two different locations in the trains station have been tested.

2.3 Test Results in Location 1

In the first location, as illustrated by Figure 2-2 the targeted zone was a desk located next to a ticket distributer. The desk is used by travelers and it is blocked from the LoS by the ticket distributer. The RIS is placed in a LoS position with the access point and it is covered by beam number 20 (which is the BS beam pointing at the RIS), with reference receive signal power (RSRP) of around -69 dBm. The RIS is around 22 m away from the BS, and around 4.5 m away from the targeted spot (the smartphone location).

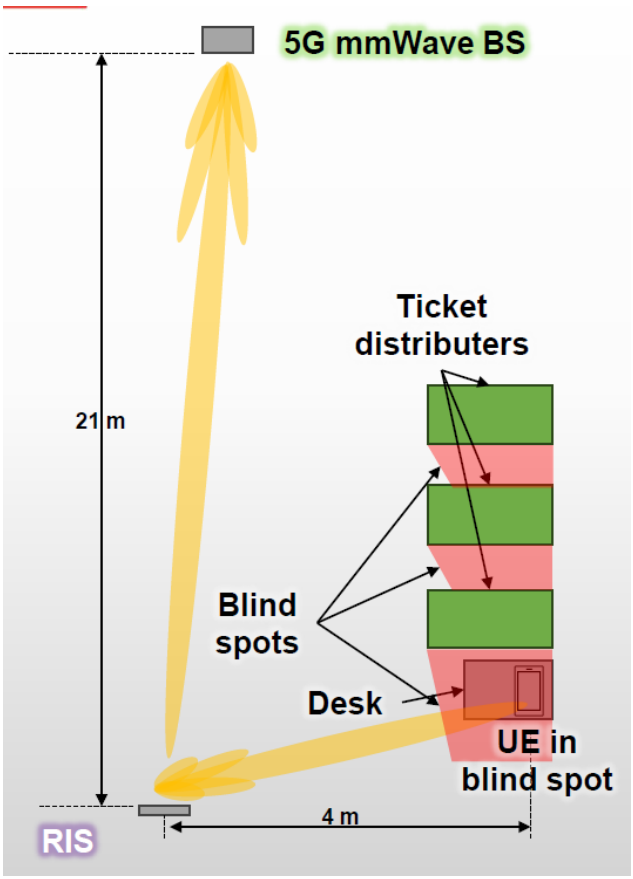

Figure 2-2 Location 1 setup.

	Without RIS	With RIS
Beam number 20	Absent	Present
RSRP of Beam 20	-93 dBm	-76 dBm **(17 dB boost)**
Throughput	493.06 Mbps	511 Mbps

Table 2-2: Results at location 1.

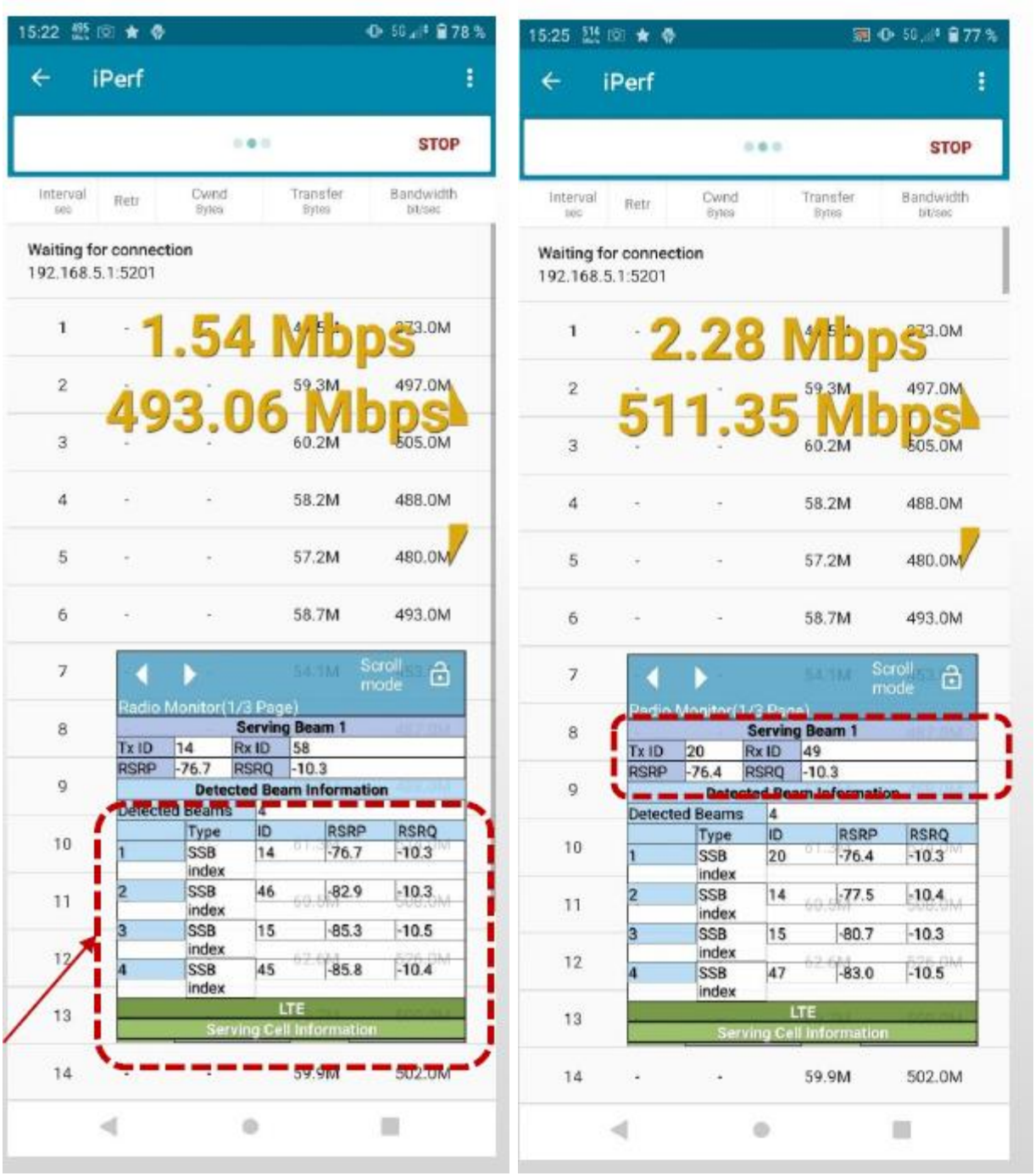

a) Without RIS (beam 20 is not part of the list)

b) With RIS (beam 20 is part of the list)

Figure 2-3 Smartphone device traces, (a) without RIS, (b) with RIS.

Results reported in Table 2-2 and Figure 2-3 show that an RSRP boost of around 17 dB, translates into a throughput boost of more than 4%. This is due to the fact that, even though the direct path is blocked, the received signal to noise ratio is high, and high modulations are already attained, even in the absence of RIS.

2.4 Test Results in Location 2

In Location 2, as illustrated by Figure 2-4, the targeted zone is an area in front of a store. The store walls are metallic and shadow the inside of the store as well as the area in front of it. The store serves travelers waiting for their trains. The RIS is placed in a LoS position with the access point and it is covered by beam number 13, with RSRP of around -71 dBm. The RIS is around 32 m away from the BS, and around 2.5 m away from the targeted spot (smartphone location).

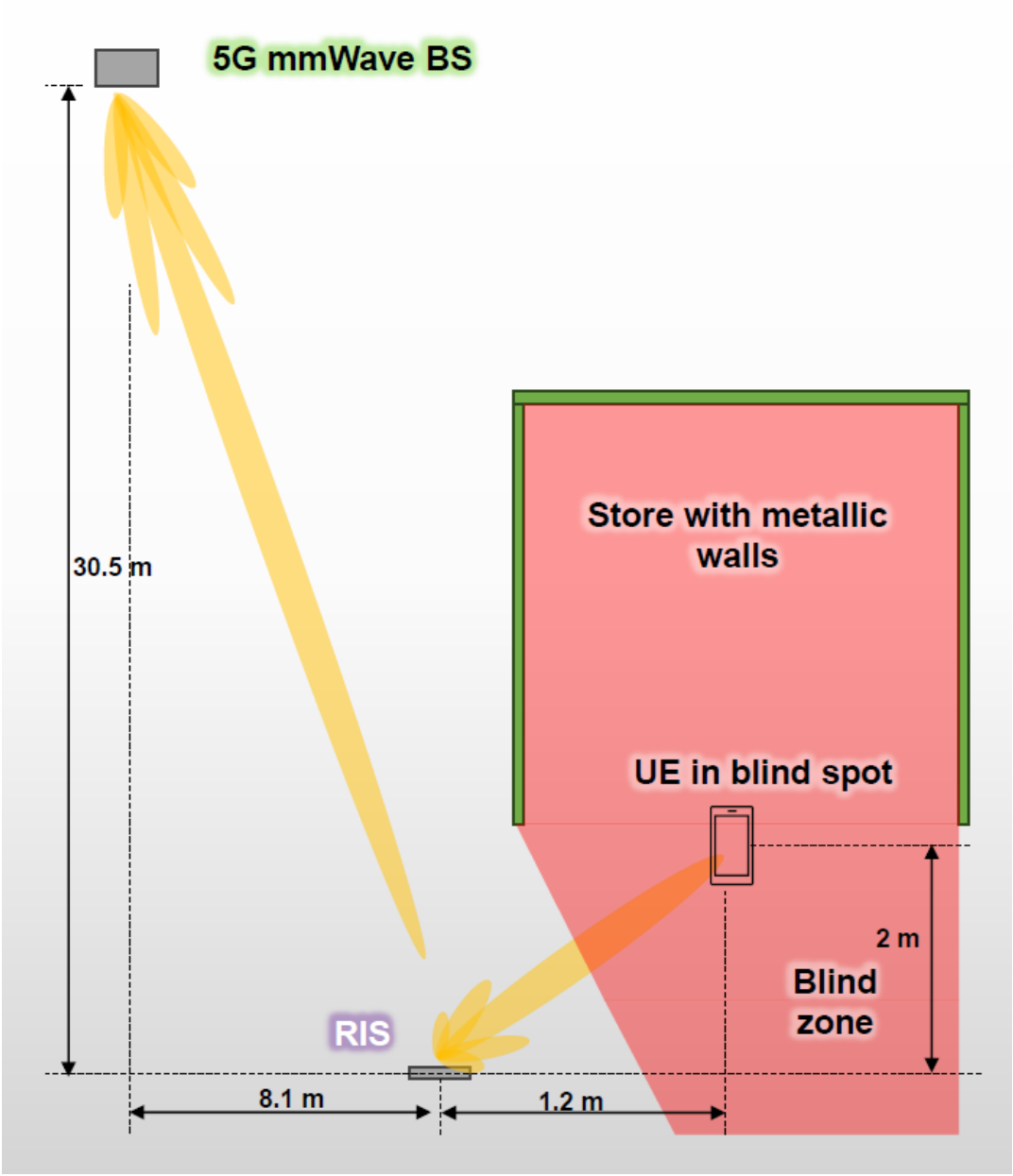

Figure 2-4 Location 2 setup.

	Without RIS	With RIS
Beam number 13	Absent	Present
RSRP of Beam 13	-94 dBm	-72 dBm **(22 dB boost)**
Throughput	332 Mbps	513 Mbps **(54% boost)**

Table 2-3: Results at location 2

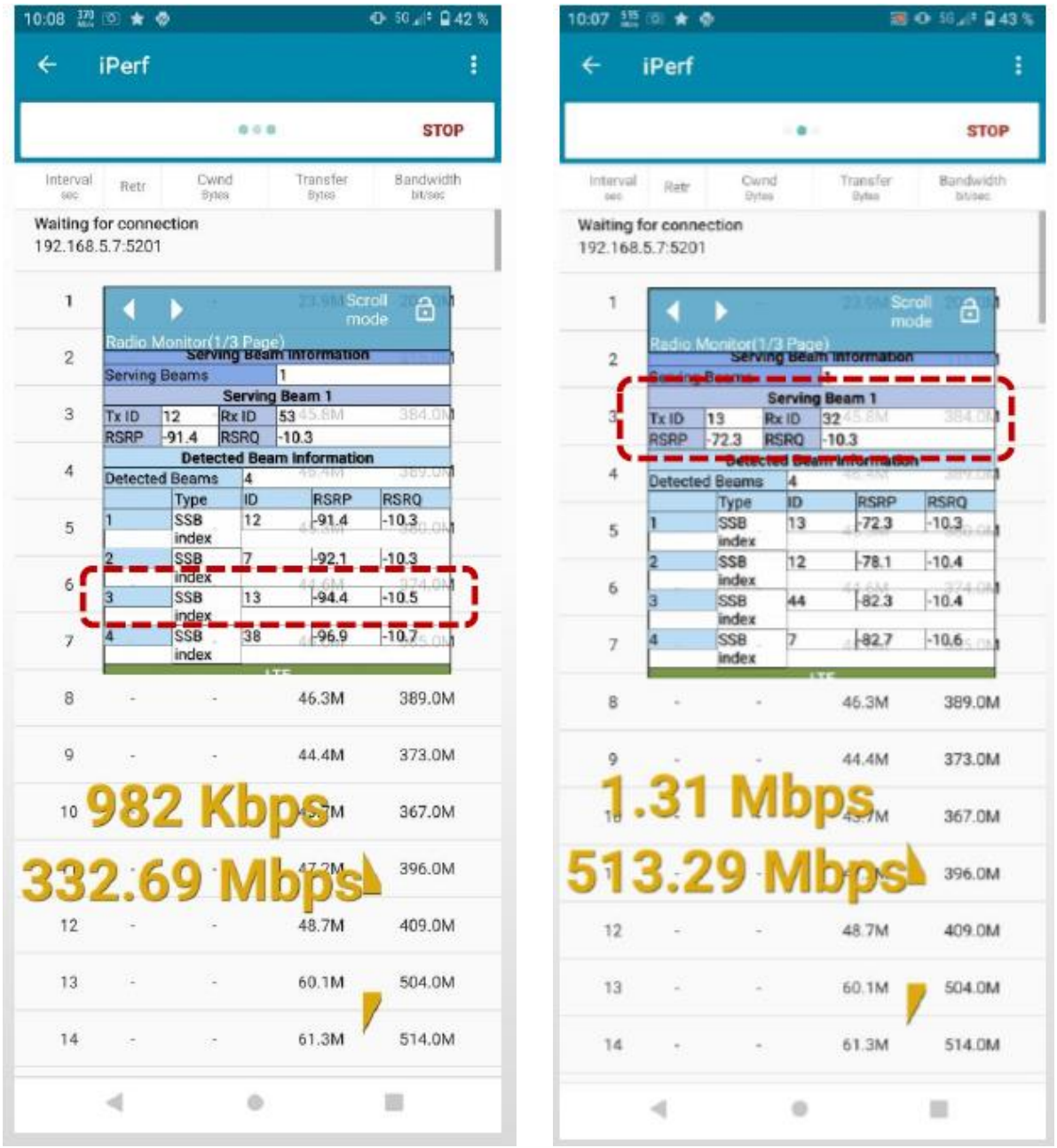

(a) Without RIS (b) With RIS

Figure 2-5 Smartphone traces in location 2.

Results reported in Table 2-3 and Figure 2-5, show that an RSRP boost of around 22 dB translates into a throughput boost of more than 50%. Again, even though the direct path is blocked, the received signal to noise ratio is high, and high modulations are already attained, even in the absence of RIS.

Figure 2-6 below plots the bit rate, RSRP and Beam indexes as seen by the smartphone. When the RIS is "off" (i.e. all unit cells in same state), the propagation channel is dominated by multipath, and the Nokia BS switches between many different beams very fast. When the RIS is 'On' and provides a strong reflected path between the BS and the smartphone, the Nokia BS selects the beam that points at the RIS and remains stable. Therefore, one additional advantage of the RIS is that it provides **stability** in the propagation channel.

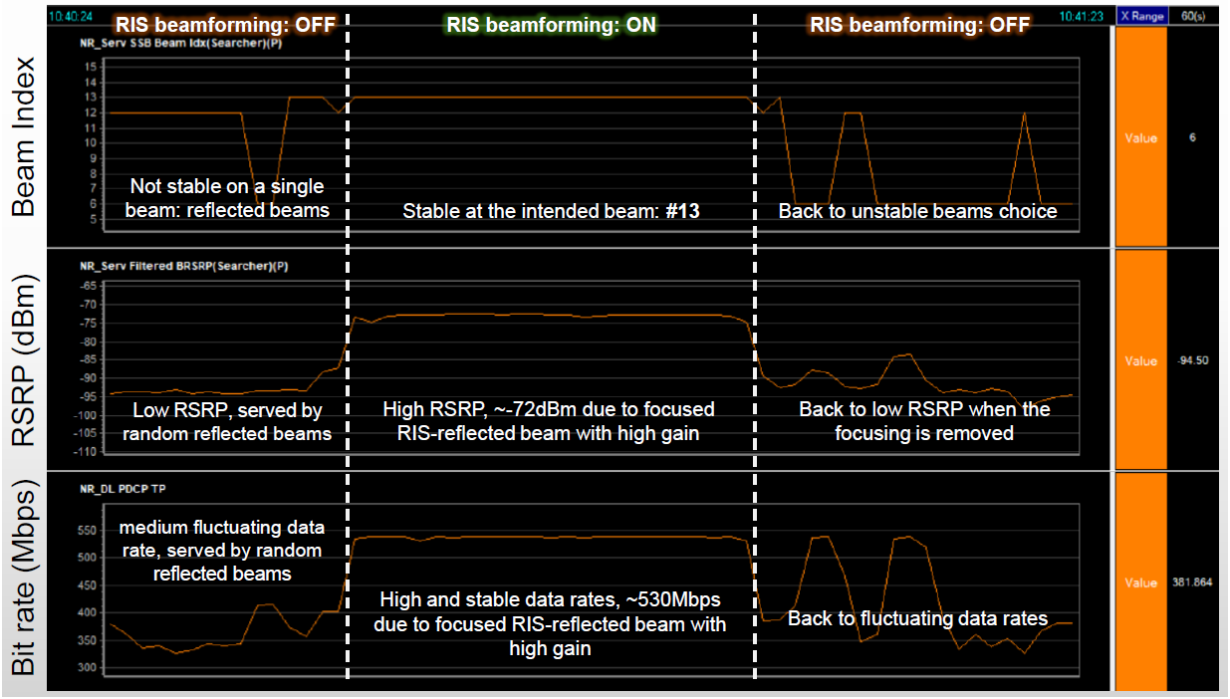

Figure 2-6 Smartphone traces in location 2 versus time (lower part: bit rate, middle part: RSRP, upper part: Beam index).

Figure 2-7 plots the variation of RSRP around the target point depending on two different setting of the RIS reflected BF tuning mechanism. A tuning with a 3° beamwidth (of the reflected beam) and a tuning of 6° are compared. As illustrated by the results, using a very narrow reflected beam of 3° provides a stronger RSRP booth at the expense of robustness in the spatial domain. Another advantage of the RIS, is that the **propagation channel spatial coherence becomes tunable**, and can be enlarged, for instance for mobility scenarios.

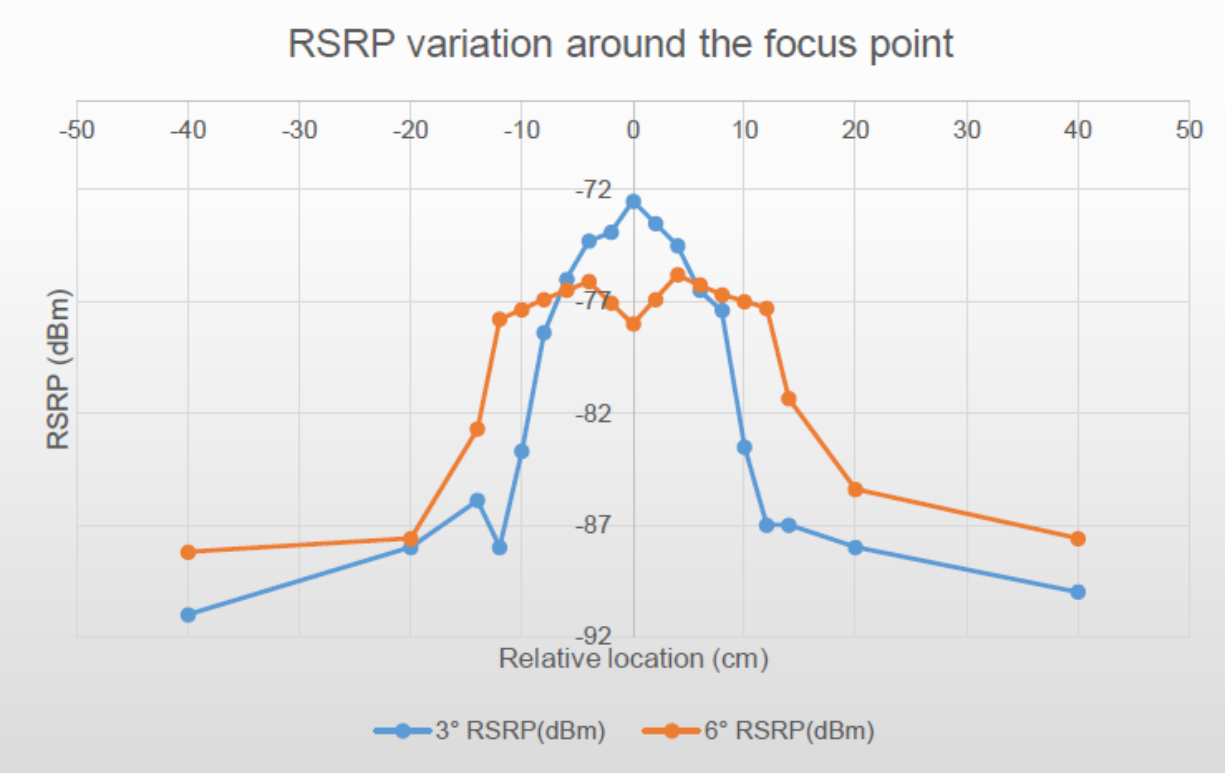

Figure 2-7 RSRP variations around the focus point for 3° and 6° RIS reflected beamwidth.

2.5 Conclusions

It has been shown that even without the commercial 5G network and 5G smartphones being aware of the RIS, the RIS already brings a significant gain of around 20 dB in RSRP. A joint optimization of the BS transmits BF with the RIS tuning, based on smartphone feedback, as in WP4, WP5 and WP6 schemes listed in [D4.4] [D4.6], **would provide even further gains**.

Additionally, during these experiments, the RIS provided a reflected beam to the target device without causing interferences to other devices on the experimental setup.

As the RIS is very low power it could operate on battery during the trial, which is to our knowledge, **a 1st in the world.**

3 Enabling a RIS-based localisation procedure in a factory environment served by a commercial 5G network operating at mmWaves

This section reports the trial performed at CRF premises aimed at validating a RIS-based localisation procedure in factory environment served by commercial 5G network. A video which summarizes the trial can be found at [CRFvid].

3.1 Setup

The trial took place at Centro Ricerche Fiat (CRF) premises in Orbassano (Torino, Italy). Experiments were conducted in the emulated factory environment, whose map presented in Figure 3-1 shows colored rectangles to delimit different subareas in which the various components involved in the experiments have been set up. Figure 3-1 shows colored rectangles to delimit different subareas in which the various components involved in the experiments have been set up.

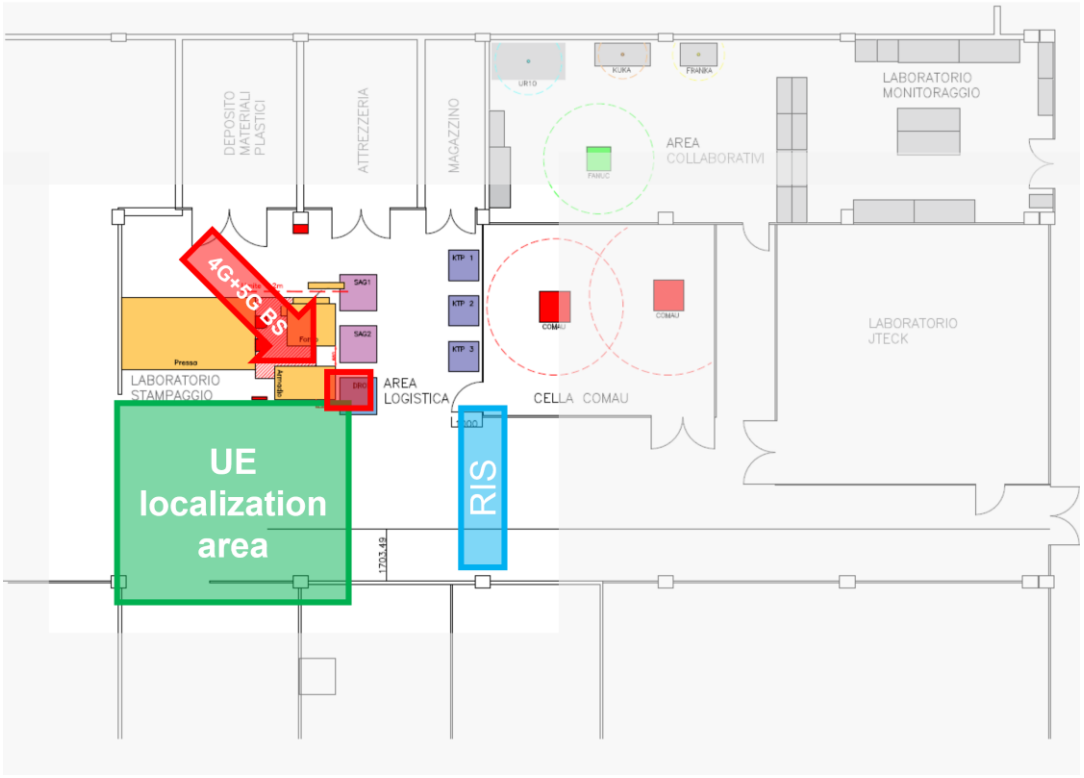

Figure 3-1 The map of the emulated factory environment at CRF premises where the main subareas involved in the trial are emphasised.

The very same colors of Figure 3-1 are recalled by the frames of the photos shown in Figure 3-2, where the very same subareas and all the main elements of the equipment used in the trial and described hereinafter can be identified in Figure 3-2, where the very same subareas and all the main elements of the equipment used in the trial and described hereinafter can be identified.

Figure 3-2 The main subareas involved in the trial together with the main elements of the equipment used.

Specifically for the trial, TIM installed a commercial 5G mmWave base station (BS):an Ericsson non standalone (NSA) gNodeB, model AIR 5322, operating at 27 GHz (FR2 spectrum licensed to TIM), with a 4G anchor operating at 1800 MHz (see Figure 3-3). It was installed on a mast at about 5.5 m from the ground and it was configured to transmit at max 10 W. Among the 24 broadcast beams available (CM2 configuration) spanning over a coverage angular area of ± 60° in azimuth and ± 15° in elevation, beam n. 2 was selected as the most suitable one to the purpose of the trial and kept constant for its whole duration.

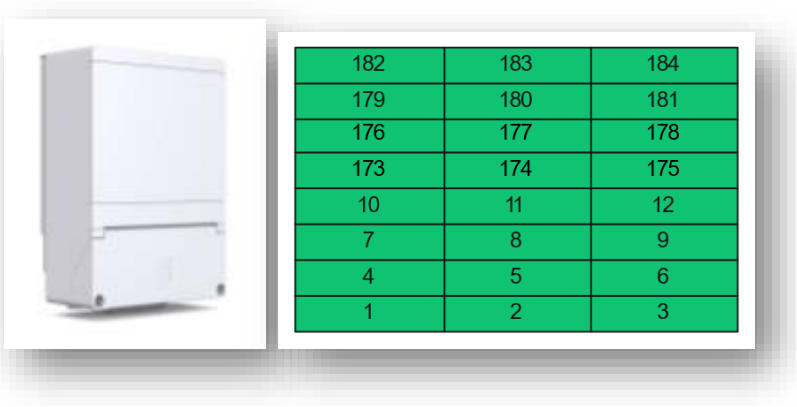

182	183	184
179	180	181
176	177	178
173	174	175
10	11	12
7	8	9
4	5	6
1	2	3

Figure 3-3 *Ericsson* mmWave AIR5322 gNodeB with the table of the available broadcast beams of CM2 configuration.

Figure 3-4 CPE MC889A by *ZTE*.

As a User Equipment (UE), the commercial Customer Premises Equipment (CPE) MC889A by ZTE shown in Figure 3-4 was used to measure the RSRP level by means of specific Android Debug Bridge (ADB) commands. The device was installed on board of an Autonomous Guided Vehicle (AGV) by OMRON.

Figure 3-5 One of the two RISs by GNW used in the trail.

Two mmWave RISs with an operating bandwidth compatible with the spectrum of the 5G commercial network were provided by GNW (see Figure 3-5). Before using the commercial CPE, a CA500 signal analyzer by *Viavi* was exploited with the aim of checking the power level of the 5G signal received at both the RISs and the receiver surfaces and the volume around them. Note that GNW RISs were characterised in detail and tested in lab in an indoor environment with controlled sources, within WP3 activities, in preparation of this trial (see [D3.1], [D3.2] and [D3.4] for details).

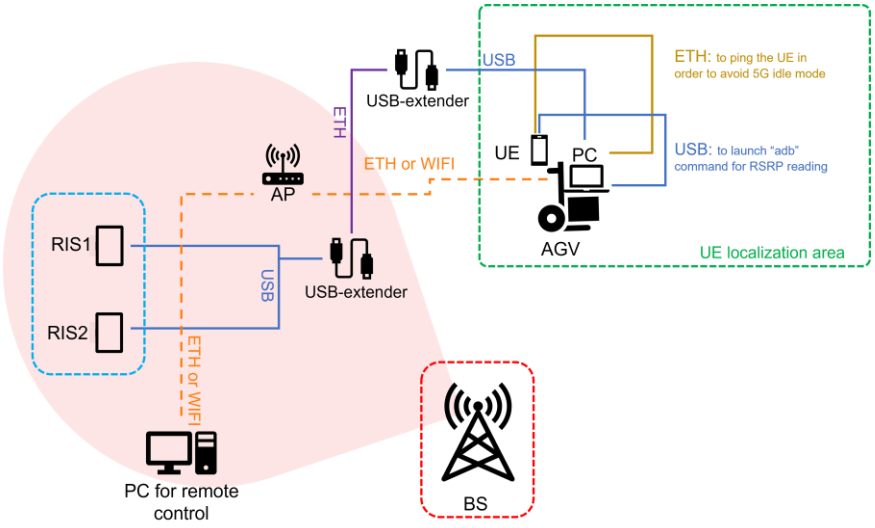

Figure 3-6 The trial setup scheme with all necessary element-to-element connections.

Both RISs and the CPE were connected to a laptop PC positioned on board the AGV. By means of a remote connection to this laptop, it was possible

- to access the received power measured by the CPE,
- to control the configuration of each RIS with a specific software provided by GNW
- to manage the whole localisation process.

Figure 3-6 sketches the setup scheme with all necessary element-to-element connections.

3.2 Objective, use case and methodology

The objective of this experiment was to validate the RIS-based localisation process described in detail in section 5.2.1 of [D5.3] entitled "RIS-aided Single-BS localisation with commercial network and equipment in a factory environment at 27 GHz".

The idea behind the implemented methodology is to identify the two reflected beams (one for each operating RIS) that better point in the direction of the UE, i.e. the ones that allow to serve the UE with the highest measured RSRP level. The localisation of the UE can then be obtained by calculating the geometrical intersection of the two beams (see Figure 3-7).

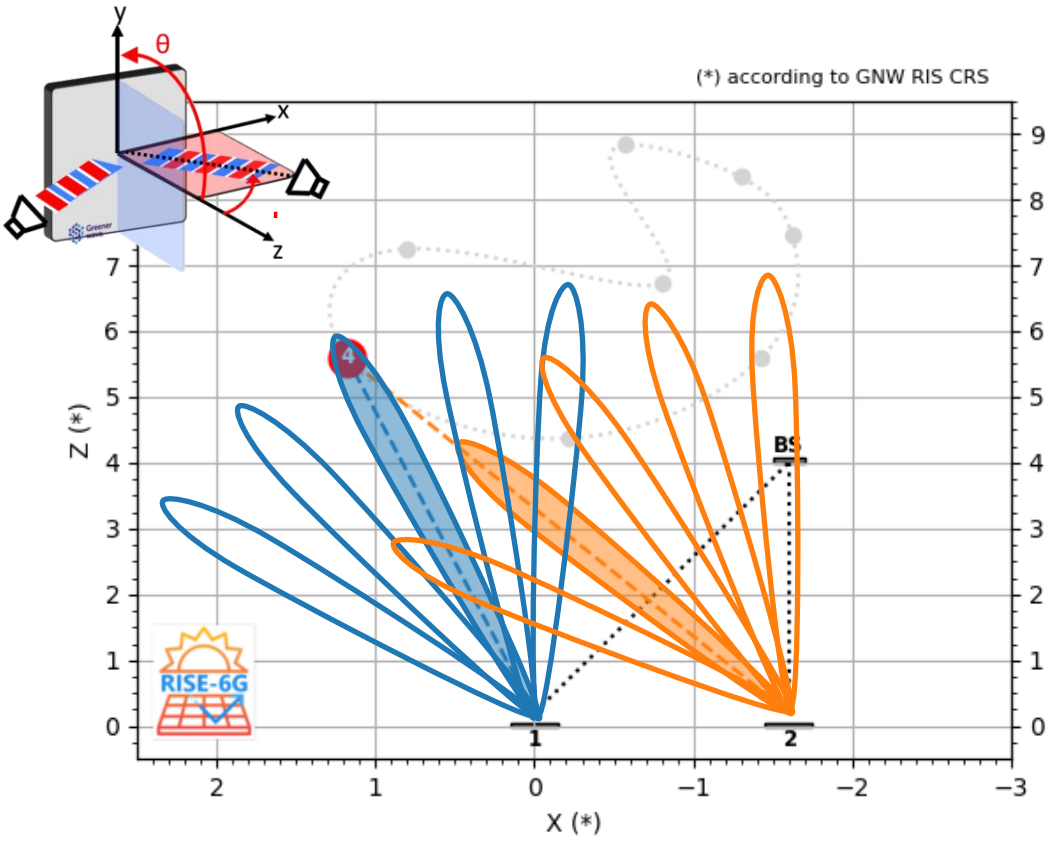

Figure 3-7 The implemented RIS-based localisation approach.

Going more into the procedural details, the localisation process consisted of the following steps:

- BS signal pointing get fixed towards the RIS devices (beam n. 2 configured)
- Optimization loop across operating RIS_x (x=1,2)
    1. non-involved RIS_y (y≠x) is configured to point reflected beams outside the UE detection area
    2. measurement loop across the set of the *n* reflection directions available for RIS_x
        a. RIS_x reflection direction (ϕ_x^n, θ_x^n) setting
        b. 5G Reference Signal Received Power ($RSRP_n$) measurement
    3. Selection of optimal (ϕ_x^{opt}, θ_x^{opt}) direction corresponding to the highest $RSRP_n$
- UE position calculation by the geometrical intersection of the selected optimal directions
- UE position estimation accuracy via laser distance meter measurements

Figure 3-8 shows an example of the outcome of the localisation process: the blue star represents the UE position identified by means of the RIS-based localisation procedure, while the yellow bullet represents the actual UE position measured by using a laser distance meter.

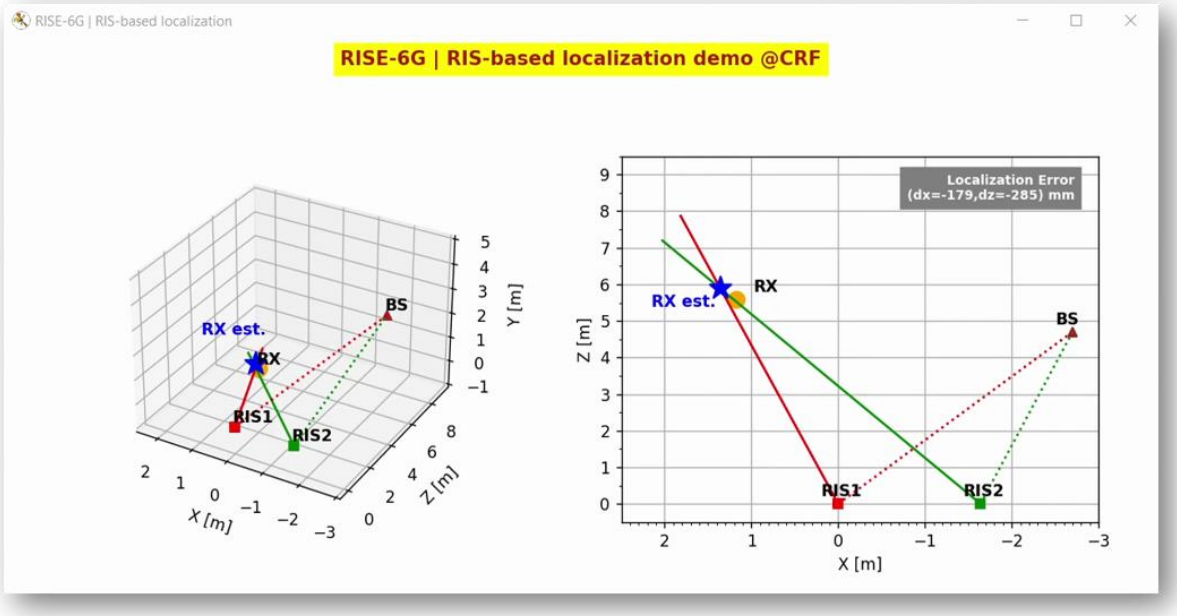

Figure 3-8 Exemplary result of the implemented RIS-based localisation process.

3.3 Test results

In order to validate the followed approach, 8 different points along the path sketched in Figure 3-7 and placed inside the UE localisation area of Figure 3-1 and Figure 3-2 were selected. For

each point, the RIS-based localisation procedure described in the previous section was run in order to localise the AGV, with the CPE on board of it.

Table 3-1 summarizes the results obtained in the trial: in particular, it reports the localisation errors both in terms of angles (azimuth and elevation) and distances (mm).

Table 3-1 – Some results from the localisation trials performed at CRF premises.

	angular values selected after RIS optimization completion									
Pos.	Phi1 [deg]	Theta1 [deg]	Phi2 [deg]	Theta2 [deg]	ΔPhi1 [deg]	ΔTheta1 [deg]	ΔPhi2 [deg]	ΔTheta2 [deg]	ΔX [mm]	ΔZ [mm]
1	-10	-5	2	-5	2,25	-1,25	1,85	-1,17	-251	-303
2	-12	-6	5	-6	2,28	-1,04	2,74	-0,88	-258	114
3	0	-8	21	-7	2,88	-1,48	3,00	-0,79	-220	98
4	13	-6	27	-6	1,10	-1,01	0,27	-1,44	-179	-285
5	9	-5	20	-5	2,70	-1,08	1,40	-1,26	-463	-727
6	-4	-5	9	-5	2,79	-0,77	1,87	-0,78	-298	-463
7	-1	-4	9	-4	2,69	-0,77	2,09	-0,78	-407	-497
8	-6	-4	4	-4	2,86	-0,61	1,67	-0,57	-315	-1030
				MIN	1,10	0,61	0,27	0,57	179	98
				AVG	2,44	1,00	1,86	0,96	299	440
				MAX	2,88	1,48	3,00	1,44	463	1030

In many cases, it can be observed that the RIS-based localisation procedure successfully identifies the UE position with an average error in the order of a few centimeters. However, in some cases, the localisation error is more significant (up to 1m), probably due to the environment characteristics around some specific positions: objects, walls and all metallic components in those parts of the localisation area cause reflections which can strongly affect the RISs localisation process operated through the implemented approach.

3.4 Conclusion

In the light of this trial, RIS-based localisation was successfully validated on-field with commercial 5G equipment.

During the experiments it was observed that, due to RIS optimization, a signal level improvement up to 20 dB, under poor coverage conditions (NLoS) could be achieved.

It is worth mentioning that multipath and scattering due to the environment, which are not tackled in currently implemented procedure, have a strong effect on the localisation accuracy and this must be taken into account for future developments of RIS-based localisation.

In addition to this, it is worth emphasizing that RIS (reflected) beam pointing angular granularity heavily impact localisation accuracy: for this reason, the three-dimensional (3D) RIS (reflected) radiation patterns knowledge plays a key role in the success of the procedure and has to be taken carefully into account in the deployment strategy.

Moreover, it is important to underline that RIS controller and localisation management functions must be currently implemented with an ad-hoc approach because, at the moment, they are not

part of any standard yet. Also, the RSRP measurement as defined by the 3rd generation partnership orject (3GPP) standard and exploited in the trial is not suited to the localisation purposes because of its slow update rate and its low resolution: new standardized techniques must be foreseen.

To conclude, despite the promising results demonstrated by this trial, it is clear that further steps are needed, both on the localisation techniques side as documented by the studies conducted within WP5 activities and on the international communication standards side, in order to provide a fully operative and usable RIS-based localisation service.

4 PoCs of RIS-aided localisation in other frequency bands

4.1 Localisation in V-band (60 GHz)

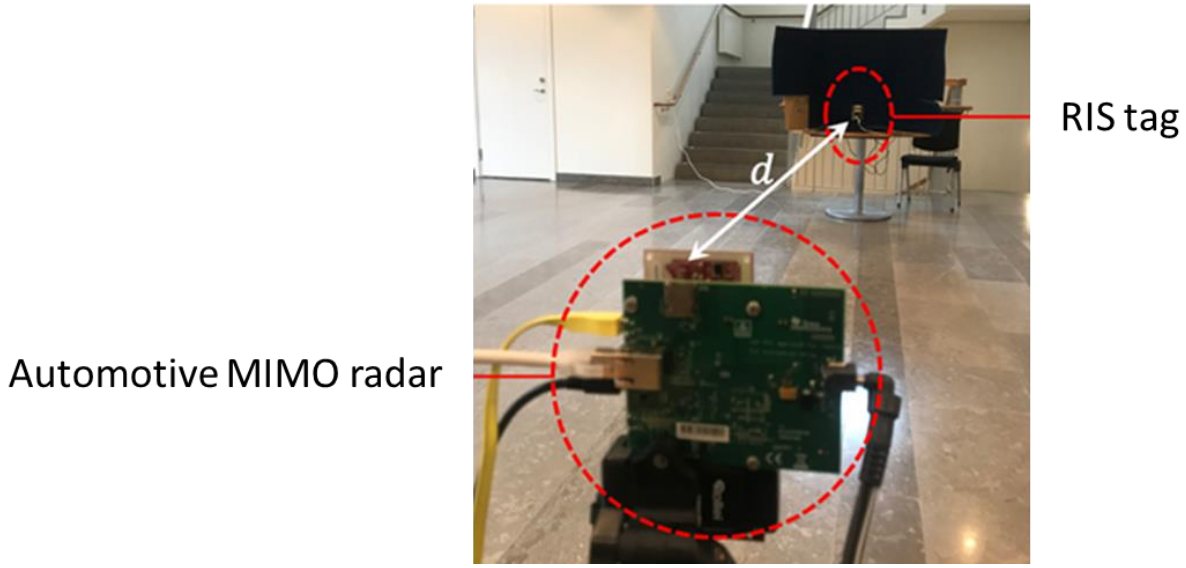

Figure 4-1 RIS PoC integration for Localisation.

The V-band RIS is also used as active tag together with commercial 60 GHz MIMO radar. When MIMO radar used indoor, multiple reflection from wall and other objects indoor creates multiple unwanted false targets which limits radar detection performance. When active RIS tag is added into the scenario as shown in Figure 4-1, the active RIS can increase the radar cross section (RCS) of the target of interesting, thus made it easier to identify this target of interest from false reflections, the active RIS can increase the RCS of the target of interesting, thus made it easier to identify this target of interest from false reflections.

The RIS is placed 4.37 meters away from the radar, and the RIS is power off and on respectively to exam the performance. The measurement plots are shown in Figure 4-2.

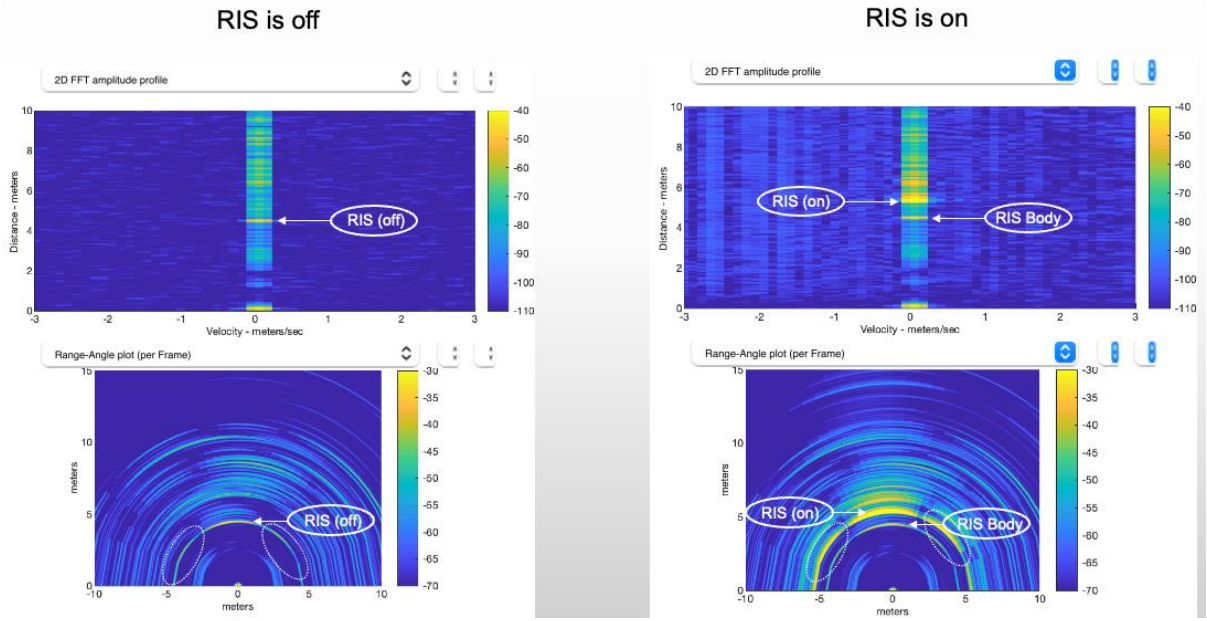

Figure 4-2 Measurement plots for V-band RIS.

It can be seen that when RIS is off, the body of the RIS can be detected however with same RCS as surrounding targets, and from two-dimensional (2D) plot it is not straightforward to identify the target. When RIS is on, The RIS acts as active reflector, due to cable delay, an additional target with 10 dB higher SNR is detected at half meter away from the RIS real position, however, the higher SNR is beneficial for separating the target from multipath reflections.

4.2 Localisation in D-band (140 GHz)

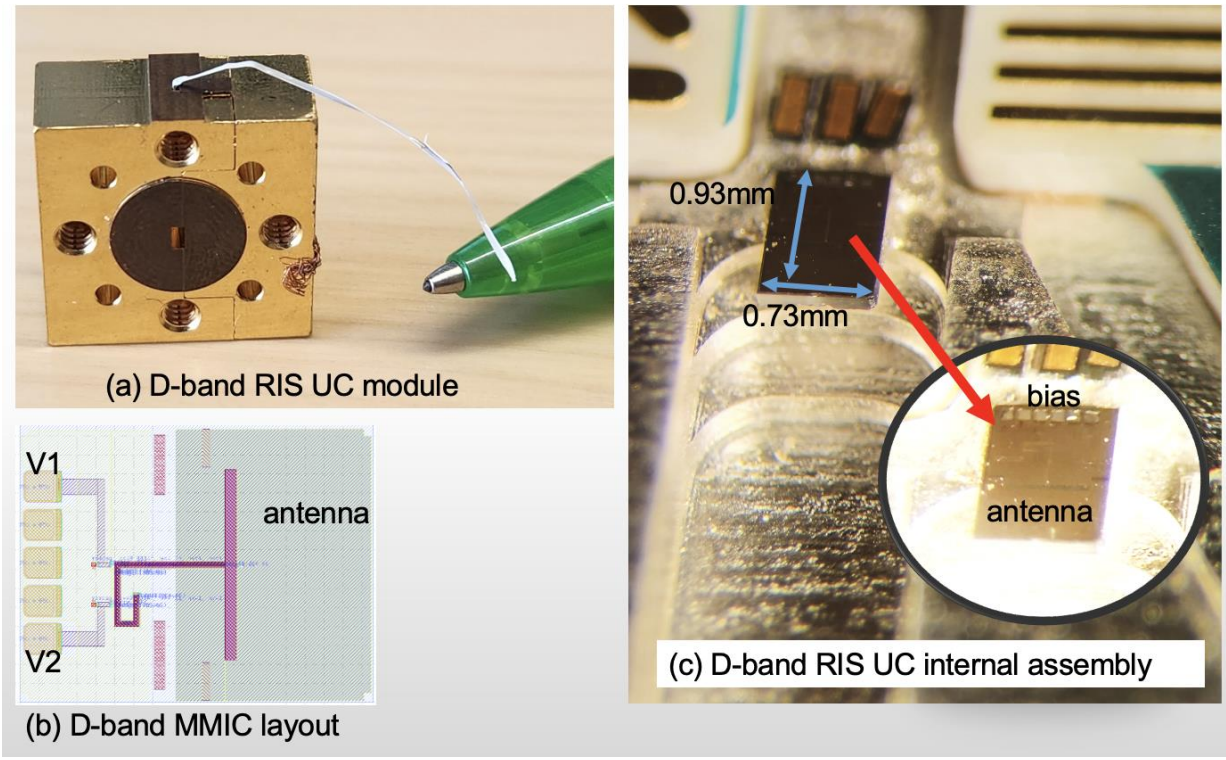

Figure 4-3 D-band RIS unit cell module, MMIC and internal assembly.

A millimeter-wave monolithic microwave integrated circuit (MMIC) is created and manufactured using a 130 nm silicon-germanium bipolar complementary metal-oxide-semiconductor (SiGe BiCMOS) process. This process incorporates an on-chip antenna, a phase shifter, and power bias pads. The MMIC is then encapsulated within a waveguide module, utilizing an open waveguide to serve as a 3 dBi antenna, functioning as a RIS unit cell module. The MMIC size is 0.93 mm by 0.73 mm, and its insertion loss and phase shifting performance is measured with control voltage from 0 to -5 V across frequency from 110 GHz to 170 GHz, the measurement result is shown in the figure below.

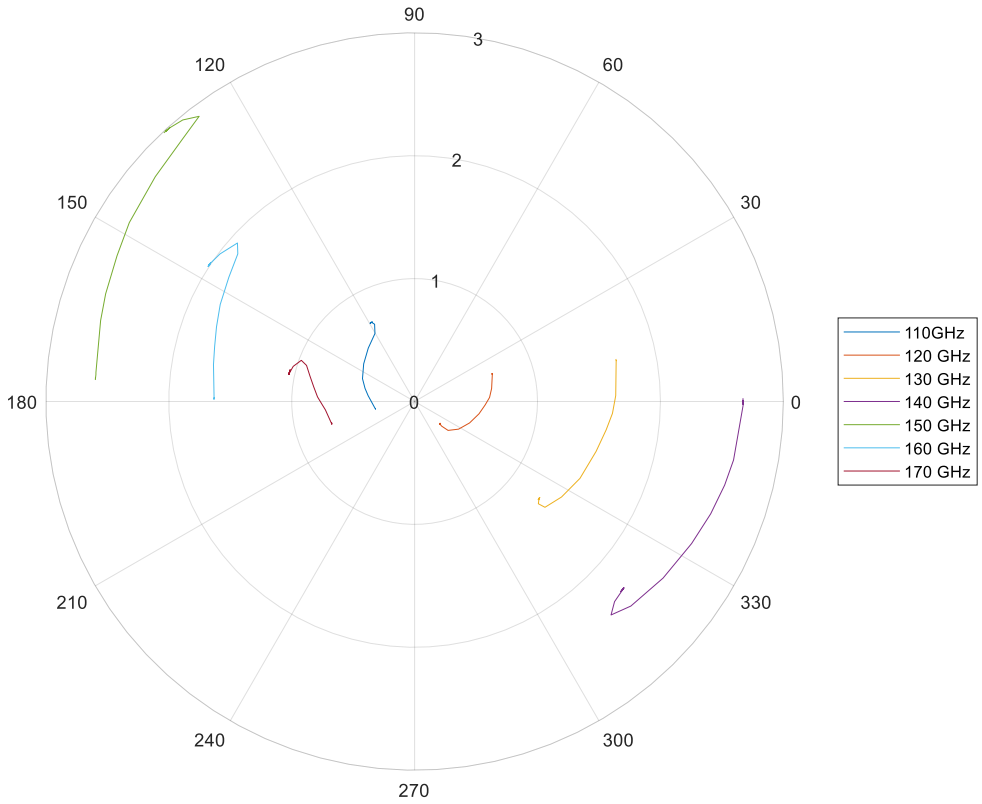

Figure 4-4 D-band RIS unit cell module, MMIC and internal assembly.

The D-band RIS UC module is used as target and commercial 120 GHz radar is used to measure the UC module. The UC module is switched between 0 and 180 deg reflection at 10 KHz thus corresponding to different phase modulation at each radar chirp frame. The setup is shown in the figure below.

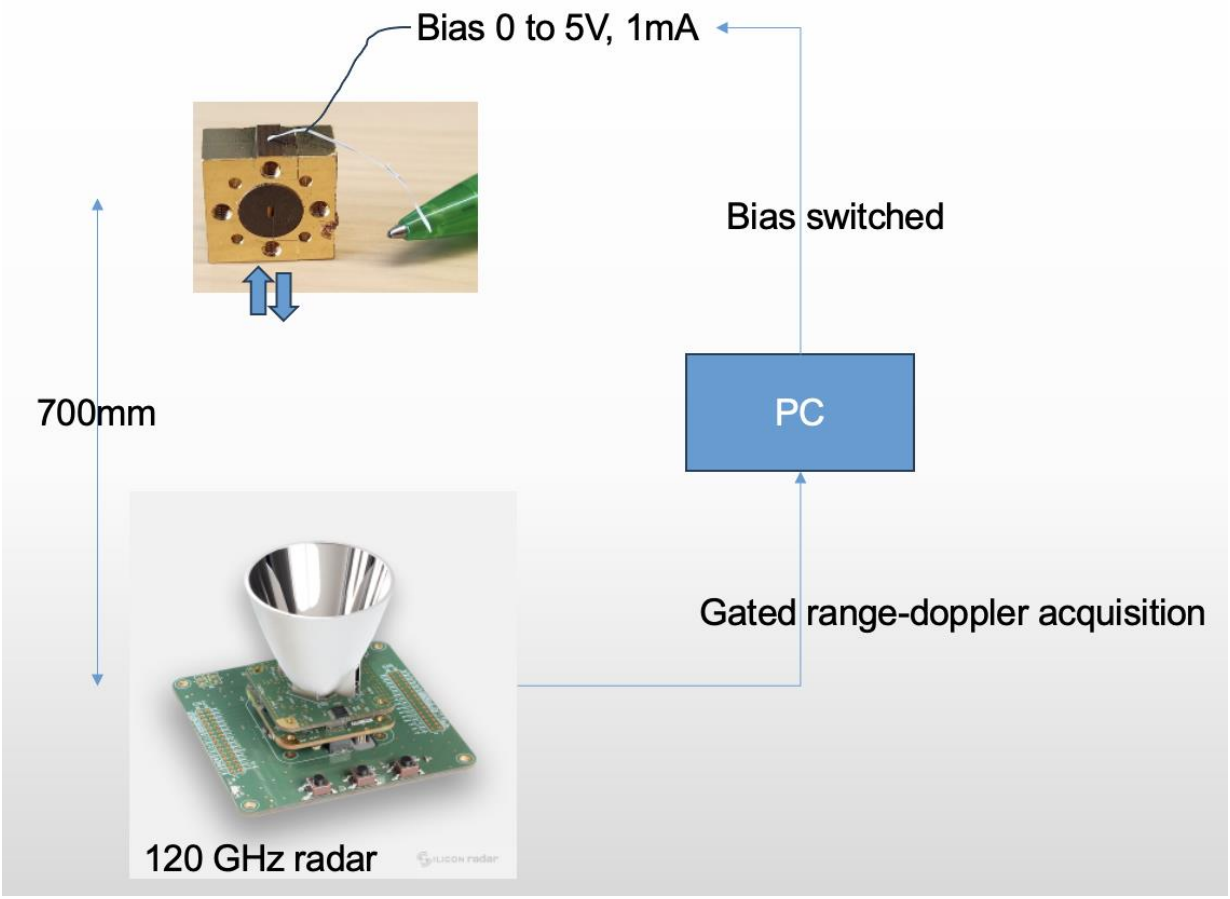

Figure 4-5 Setup.

Measurement results on the left figure of Figure 4-6 show 50 frames acquisition with UC at 70 cm without bias modulation, it can be seen the noise background is on the level of -130 dB with SNR about 28 dB. On the right hand, RIS is modulated at the same distance and also 50 frames, due to the phase modulation, the background noise is suppressed and background is reduced to -150 dB which yield about 20 dB process gain on the target SNR.

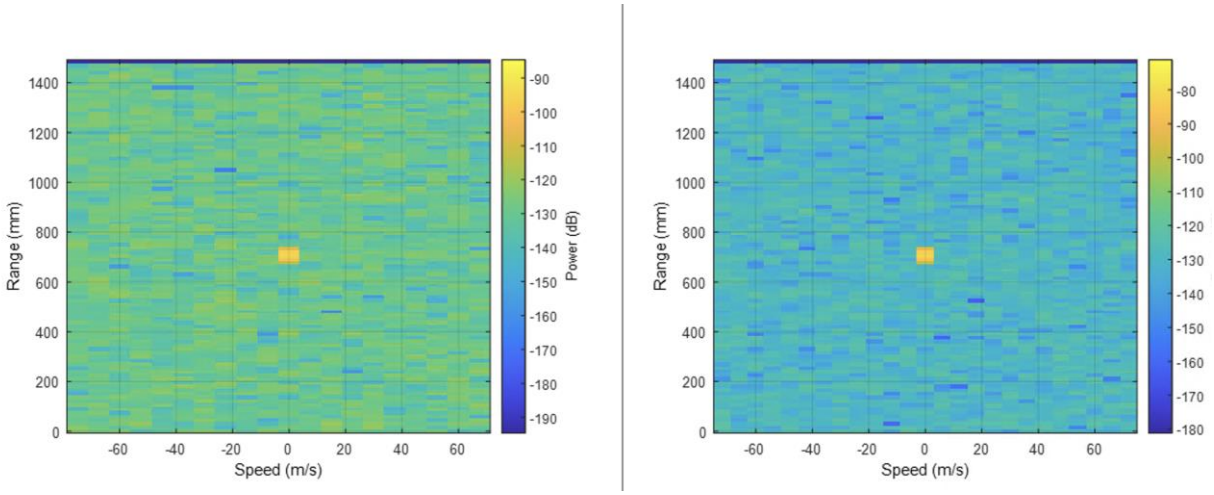

Figure 4-6 Target enhancement using RIS UC with phase modulation.

5 Energy Consumption and Sustainability aspects, based on RIS prototypes.

5.1 Energy Consumption of RIS prototypes

The RIS used during the trial was battery powered during the trial. The RIS consumes 2 watts, 18 watts and 35 watts, in idle mode, average and at maximum, respectively. However, new prototypes with ten times (or even more) lower energy consumption are being built. We can therefore expect that the future RIS products consumption will be **in the order or even below 1 watt**.

We also provide hereafter a tentative analysis of a varactor-based R-RIS energy consumption based on a prototype developed by Orange and detailed in [PSPH+23]. The studied RIS prototype, is composed of 984 unit-cells, and operates in the 5.15-5.35 GHz band. The phase-shift of each unit-cell is controlled individually and continuously through four varactors by applying a voltage to the varactors (the detailed design of the unit cell is given in [BPB+18][PBF+13]). Each unit-cell alone needs a Femto Ampere of current and up to 5 Volts, hence, up to 5 femto Watt per unit-cell. The RIS has close to 1000 unit-cells. Therefore, the total energy consumption due to unit-cell varactors alone, is in the order of picowatt. One must add the energy necessary to control the circuit to send orders (i.e., in the micro-controller to generate the voltages in the digital domain and in the digital analog converters (DACs) to convert the voltages in the digital domain into the analog domain, etc.) to this energy consumption. Again, we expect that, with an integrated design of the control circuit, the total RIS consumption would remain **in the order or even below 1 watt**.

5.2 Comparison with existing active equipments

This section compares the estimated energy consumption of RIS devices with the ones of existing active radio equipments such as with active relays, small cells etc. A Wi-Fi router typically uses 2 to 20 watts depending on the product based on published benchmarks ([ben1[ben2][ben3]]). One can assume that a good-quality Wi-Fi router consumes around **10 watts** in average.

Analysis from Sub-Sections 5.1 therefore show **an energy consumption reduction factor of one order of magnitude**. Such numbers will help updating the parameters of system level energy-efficiency models such the ones developed in [MDR19] [HZA+19] and [D2.4].

5.3 Sustainability: building RIS by refurbishing antennas

We want to emphasize that one of the RIS prototypes described in Section 5.1 and detailed in [PSPH+23] is an example of **low carbon-footprint** RIS building, thanks to the **refurbishing** of an antenna. The RIS was a novel equipment equipment that has been fabricated **with minimum energy footprint and environmental impact** by refurbishing an existing radio equipment. Indeed, the RIS prototype illustrated by Figure 5-1 b) results from the refurbishing of a Reflect Array antenna [BPB+18] [PBF+13] (illustrated by Figure 5-1 a)) with 3D transmit BF capability. During this refurbishing step, the unit-cells and the control circuit were kept, whereas the transmit RF chain has been withdrawn. Figure 5-1 c) illustrates the compact electronic control circuit allowing for an independent control of each of the 984 unit cells. To achieve such challenge, the control has been split into four different circuits, each controlling a distinct quarter of 246 different unit-cells.

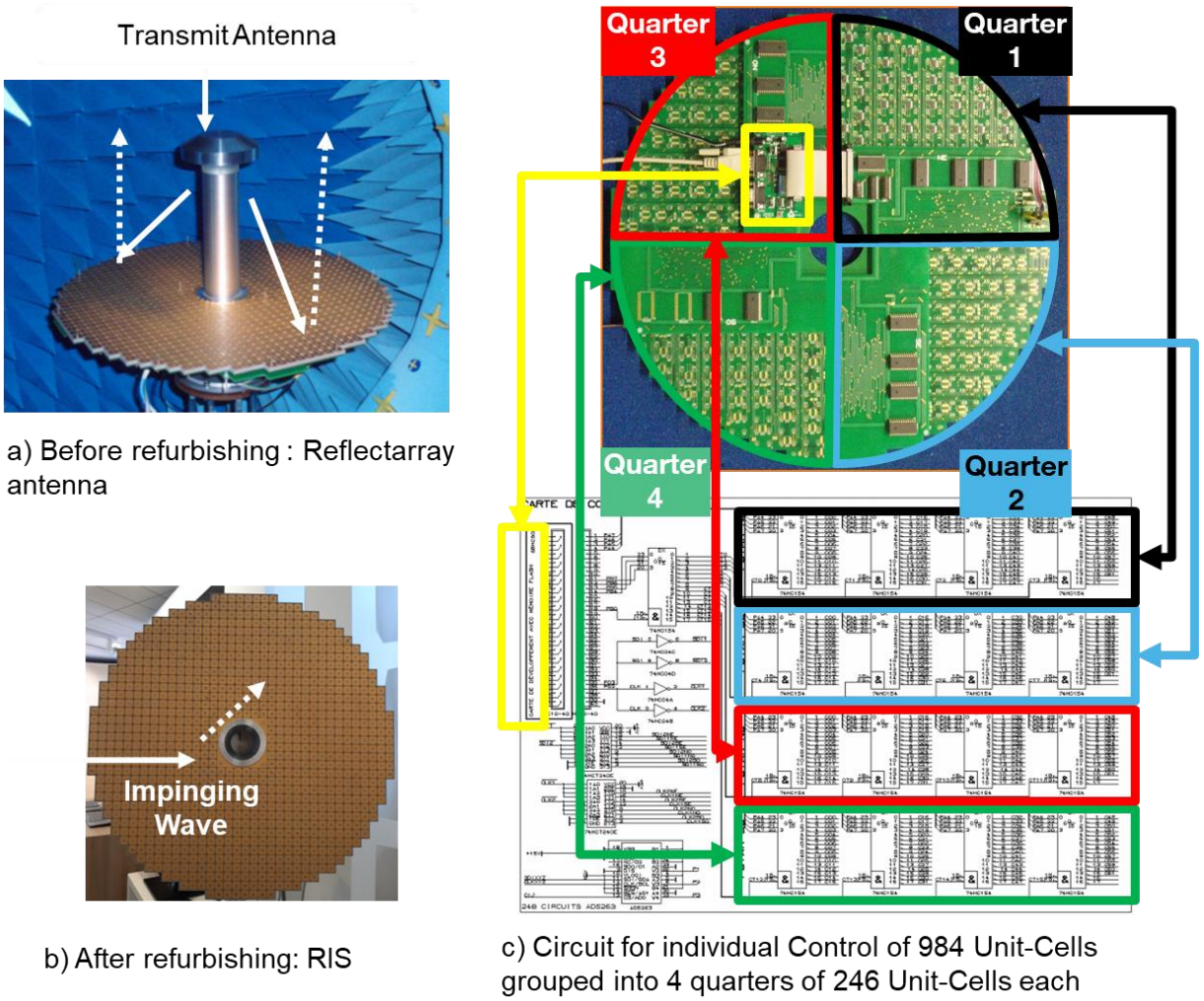

a) Before refurbishing : Reflectarray antenna

b) After refurbishing: RIS

c) Circuit for individual Control of 984 Unit-Cells grouped into 4 quarters of 246 Unit-Cells each

Figure 5-1 Low carbon-footprint RIS prototype building, thanks to refurbishing.

6 Conclusions and outlook

In this deliverable, we have presented the final results on RIS field-trials with RIS prototypes developed by partners of the project.

A first trial has shown in Rennes SNCF Train station, that even without the Orange commercial 5G network and 5G smartphones (in the mmWave band) being aware of the RIS, the RIS could already bring a significant **gain of around 20 dB in RSRP**. This boosting could potentially also be converted into EMFEU boosting. In a second trial in a factory environment at CRF premises, RIS-based localisation was successfully validated on-field with commercial 5G equipment (in the mmWave band) operated by TIM. During the experiments it was observed that, due to RIS optimization, a signal level improvement **up to 20 dB**, under poor coverage conditions (NLoS) could be achieved. Other trials at 60 GHz and 140 GHz have tested RIS-aided localisation successfully. Also, based on the study of two prototypes (among which, one working with a battery during trials), it is likely that **future RIS prototypes will be able to operate with an order of magnitude less power than an active relay**. Additionally, a very preliminary experiment has shown that RIS can also be used to perform interference nulling and boost secrecy.

In **conclusion**, the project trials, some with RISE-6G RIS prototypes, commercial mobile network equipments and smartphones, show that RIS is a promising technology to boost connectivity and enable localization, achieving **up to 20 dB gain** of receive signal strength improvement. Regarding **outlooks**, **further steps are needed in the direction of implementation and standardisation**. Indeed, in current trials, a lot of radio optimization is performed offline and in a static manner. Innovations and techniques created in WP4, WP5 and WP6, that dynamically and jointly optimize BS transmission/reception, RIS tuning and exploiting smartphone feedbacks, will be necessary to provide a **fully operative and usable RIS-empowered networks**. Finally, more efforts are needed to produce more low-power RIS prototypes with a an order of magnitude less operating power than active relay.

7 References

[ben1]	https://energyusecalculator.com/electricity_wifirouter.htm
[ben2]	https://news.energysage.com/how-many-watts-does-a-wi-fi-router-use/
[ben3]	https://www.guru3d.com/articles-pages/asus-rt-ax88u-dual-band-ax6000-router,9.html
[BGM+15]	L. Bastianelli, L. Giacometti, V. M. Primiani and F. Moglie, "Effect of absorber number and positioning on the power delay profile of a reverberation chamber," 2015 IEEE International Symposium on Electromagnetic Compatibility (EMC), 2015, pp. 422-427, doi: 10.1109/ISEMC.2015.7256199.
[BMB+17]	M. Barazzetta et al., "A Comparison Between Different Reception Diversity Schemes of a 4G-LTE Base Station in Reverberation Chamber: A Deployment in a Live Cellular Network," in IEEE Transactions on Electromagnetic Compatibility, vol. 59, no. 6, pp. 2029-2037, Dec. 2017, doi: 10.1109/TEMC.2017.2657122.
[BMD+17]	M. Barazzetta, D. Michel, R. Diamanti, L. Bastianelli, F. Moglie and V. M. Primiani, "Optimization of 4G wireless access network features by using reverberation chambers: Application to high-speed train LTE users," 2016 46th European Microwave Conference (EuMC), 2016, pp. 719-722, doi: 10.1109/EuMC.2016.7824444.
[BMG+14]	M. Barazzetta, D. Micheli, P. Gianola, F. Moglie and V. Mariani Primiani, "4G-LTE base station output power estimation from statistical counters during over-the-air tests in reverberation chamber," 2014 International Symposium on Electromagnetic Compatibility, 2014, pp. 284-289, doi: 10.1109/EMCEurope.2014.6930918.
[BPB+18]	J. M. Baracco, P. Ratajczak, P. Brachat, J.M. Fargeas, G. Toso, “Reconfigurable Antennas Demonstrators Using Varactors Technology,” in Proc. 39th ESA Antenna Wksp. Innovative Antenna Systems and Technologies for Future Space Missions, 2–5 Oct. 2018, ESA/ESTEC, Noordwijk, The Netherlands
[CDB+23]	M. Colombo, R. Diamanti, L. Bastianelli, G. Gradoni, E. Colella, V. Mariani Primiani, F. Moglie and D. Micheli, "Experimental Investigation of 5G Base Station Functionalities in Reverberation Chamber at Millimeter-Wave," in IEEE Access, vol. 11, pp. 121702-121711, 2023, doi: 10.1109/ACCESS.2023.3328583.
[D2.4]	RISE-6G Deliverable D2.4 “Metrics and KPIs for RISE wireless systems analysis: final results”, Feb. 2022.
[GHR+10]	E. Genender, C. L. Holloway, K. A. Remley, J. M. Ladbury, G. Koepke and H. Garbe, "Simulating the Multipath Channel With a Reverberation Chamber: Application to Bit Error Rate Measurements," in IEEE Transactions on Electromagnetic Compatibility, vol. 52, no. 4, pp. 766-777, Nov. 2010, doi: 10.1109/TEMC.2010.2044578.
[GLL+22]	J.B. Gros, G. Lerosey, F. Lemoult, M. Lodro, S. Greedy, and G. Gradoni. “Multi-path fading and interference mitigation with Reconfigurable Intelligent Surfaces.” https://arxiv.org/abs/2206.08290
[HZA+19]	C. Huang, A. Zappone, G. C. Alexandropoulos, M. Debbah and C. Yuen, "Reconfigurable Intelligent Surfaces for Energy Efficiency in Wireless

	Communication," in IEEE Transactions on Wireless Communications, vol. 18, no. 8, pp. 4157-4170, Aug. 2019, doi: 10.1109/TWC.2019.2922609. Available at: https://arxiv.org/pdf/1810.06934.pdf
[LGG+22]	M. Lodro, J.B. Gros, S. Greedy, G. Lerosey, A. Al Rawi, and G. Gradoni. "Experimental Evaluation of Multi-operator RIS-assisted Links in Indoor Environment." https://arxiv.org/abs/2206.07788
[MBB+20]	V. M. Primiani et al., "Reverberation chambers for testing wireless devices and systems," in IEEE Electromagnetic Compatibility Magazine, vol. 9, no. 2, pp. 45-55, 2nd Quarter 2020, doi: 10.1109/MEMC.2020.9133241.
[MBC+16]	D. Micheli, M. Barazzetta, C. Carlini, R. Diamanti, V. M. Primiani and F. Moglie, "Testing of the Carrier Aggregation Mode for a Live LTE Base Station in Reverberation Chamber," in IEEE Transactions on Vehicular Technology, vol. 66, no. 4, pp. 3024-3033, April 2017, doi: 10.1109/TVT.2016.2587662.
[MBD+18]	D. Micheli et al., "Over-the-Air Tests of High-Speed Moving LTE Users in a Reverberation Chamber," in IEEE Transactions on Vehicular Technology, vol. 67, no. 5, pp. 4340-4349, May 2018, doi: 10.1109/TVT.2018.2795650.
[MBM+15]	D. Micheli, M. Barazzetta, F. Moglie and V. Mariani Primiani, "Power Boosting and Compensation During OTA Testing of a Real 4G LTE Base Station in Reverberation Chamber," in IEEE Transactions on Electromagnetic Compatibility, vol. 57, no. 4, pp. 623-634, Aug. 2015, doi: 10.1109/TEMC.2015.2434277.
[MDB+23]	D. Micheli et al., "Test of 5G System in the Reverberation Chamber at mm-wave," 2023 17th European Conference on Antennas and Propagation (EuCAP), Florence, Italy, 2023, pp. 1-4, doi: 10.23919/EuCAP57121.2023.10133586.
[MDR19]	M. Di Renzo et al, "Reconfigurable Intelligent Surfaces vs. Relaying: Differences, Similarities, and Performance Comparison" EURASIP JWCN 2019. Available at: https://arxiv.org/pdf/1908.08747.pdf
[MDS+21]	P. Mursia, F. Devoti, V. Sciancalepore and X. Costa-Pérez, "RISe of Flight: RIS-Empowered UAV Communications for Robust and Reliable Air-to-Ground Networks," in *IEEE Open Journal of the Communications Society*, vol. 2, pp. 1616-1629, 2021.
[MFC+21]	E. Moro, I. Filippini, A. Capone and D. De Donno, "Planning Mm-Wave Access Networks With Reconfigurable Intelligent Surfaces," *2021 IEEE 32nd Annual International Symposium on Personal, Indoor and Mobile Radio Communications (PIMRC)*, 2021, pp. 1401-1407.
[MSG+21]	P. Mursia, V. Sciancalepore, A. Garcia-Saavedra, L. Cottatellucci, X. C. Pérez and D. Gesbert, "RISMA: Reconfigurable Intelligent Surfaces Enabling Beamforming for IoT Massive Access," in *IEEE Journal on Selected Areas in Communications*, vol. 39, no. 4, pp. 1072-1085, April 2021, doi: 10.1109/JSAC.2020.3018829.
[RBF+13]	P. Ratajczak, P. Brachat, J-M Fargeas, J-M Baracco, "C-Band Active Reflectarray Based on High Impedance Surface," in Proc. 2013 IEEE Int'l. Symp. Phased Array Systems and Technology, Waltham, MA, 2013, pp. 570–76.
[RBS+23]	Philippe Ratajczak, Ramiz Bennadji, Eric Séguenot, Dinh-Thuy Phan-Huy "Experimental Demonstration of Reflected Beamforming and Interference Nulling

	at sub6GHz thanks to Varactor Based Reconfigurable Intelligent Surface", submitted to Annals of Telecommunications on 21 December 2023. Available soon on arxiv.
[RS+23]	P. Ratajczak, S. Séguenot, D.-T. Phan Huy "Experimental Demonstration of 3D Reflected Beamforming at sub6GHz thanks to Varactor Based Reconfigurable Intelligent Surface," in Proc. International Conference on 6G Networking (6Gnet), October 18-20, 2023, Paris, France. Available at: https://arxiv.org/ftp/arxiv/papers/2307/2307.06716.pdf
[D2.3]	H2020-ICT-52 RISE-6G, "Reference system, scenarios and use cases analysis: final results", 2022. Online at: https://rise-6g.eu/Pages/DELIVERABLES/Livrables.aspx
[D2.4]	H2020-ICT-52 RISE-6G, "Metrics and KPIs for RISE wireless systems analysis: final results", 2022. Online at: https://rise-6g.eu/Pages/DELIVERABLES/Livrables.aspx
[D3.1]	H2020-ICT-52 RISE-6G, "D3.1 - Preliminary RIS model and measurement campaigns", 2022. Online at: https://rise-6g.eu/Pages/DELIVERABLES/Livrables.aspx
[D3.2]	H2020-ICT-52 RISE-6G, "D3.2 - RIS designs, and first prototypes characterization", 2023. Online at: https://rise-6g.eu/Pages/DELIVERABLES/Livrables.aspx
[D3.4]	H2020-ICT-52 RISE-6G, 'D3.4 Optimised RIS prototypes for PoCs and model assessment test', 30/06/2023. Online at: https://rise-6g.eu/Pages/DELIVERABLES/Livrables.aspx
[D4.4]	H2020-ICT-52 RISE-6G, "Multi-user techniques and connectivity of RIS based communication and mobile edge computing (Final Specifications)", 30/06/2023. Online at: https://rise-6g.eu/Pages/DELIVERABLES/Livrables.aspx
[D5.3]	H2020-ICT-52 RISE-6G, "D5.3 - Control for RIS-based localisation and sensing (Final Specifications)", 30/06/2023. Online at: https://rise-6g.eu/Pages/DELIVERABLES/Livrables.aspx
[D5.4]	H2020-ICT-52 RISE-6G, "D5.4 - Estimation algorithms for RIS-based localisation, mapping and sensing (Final Specifications)", 30/06/2023. Online at: https://rise-6g.eu/Pages/DELIVERABLES/Livrables.aspx
[D6.4]	H2020-ICT-52 RISE-6G, "D6.4 - Sustainable RIS solutions design for EE, EMFEE and SSE (Final Specifications)", 30/06/2023. Online at: https://rise-6g.eu/Pages/DELIVERABLES/Livrables.aspx
[D7.1]	H2020-ICT-52 RISE-6G, "D7.1 - Integration methodology and impact measurements through advanced KPIs", 2022. Online at: https://rise-6g.eu/Documents/LIVRABLES/RISE-6G_WP7_D7.1_Final.pdf
[D7.2]	H2020-ICT-52 RISE-6G, "Final results on the platform integration and validation", 2023. Online at: https://rise-6g.eu/Pages/DELIVERABLES/Livrables.aspx
[RMG+22]	M. Rossanese, P. Mursia, A. Garcia-Saavedra, V. Sciancalepore, A. Asadi, and X. Costa-Perez, "Designing, Building, and Characterizing RF Switch-based Reconfigurable Intelligent Surfaces", in Proceedings of the 16th ACM Workshop on Wireless Network Testbeds, Experimental Evaluation & Characterization

	(WiNTECH'22), 2022, Sydney, NSW, Australia. [Online]: http://arxiv.org/abs/2207.07121
[RS]	Rennes station - Wikipedia. Online at: https://en.wikipedia.org/wiki/Rennes_station
[RS+23]	P. Ratajczak, S. Séguenot, D.-T. Phan Huy "Experimental Demonstration of 3D Reflected Beamforming at sub6GHz thanks to Varactor Based Reconfigurable Intelligent Surface," accepted to International Conference on 6G Networking (6Gnet), October 18-20, 2023, Paris, France. Available at: https://arxiv.org/ftp/arxiv/papers/2307/2307.06716.pdf
[WTL+22]	Jinghe Wang, Wankai Tang, Jing Cheng Liang, Lei Zhang, Jun Yan Dai, Xiao Li, Shi Jin, Qiang Cheng, and Tie Jun Cui "Reconfigurable Intelligent Surface: Power Consumption Modeling and Practical Measurement Validation", on 2022 arxiv. Available at: https://arxiv.org/pdf/2211.00323.pdf
[CRFvid]	https://youtu.be/lvSvmGSuKPk

8 Annex: A first interference nulling experiment for SSE boosting

This section summarizes some experiments reported in detail in [RBs+23]. The RIS prototype presented in Section 5.1 and detailed in [PSPH+23] has been used to perform interference nulling. Figure 8-1 a) b) c) and d) illustrate the setup. The same RIS, receiver (RX), transmitter (TX) equipments are used as in [PSPH+23]. TX and RX are directional antennas. As they are both positioned, side by side, on a wall, they have a low direction propagation path. The RIS is facing TX and RX. **Another metallic plate provides an additional reflected path** between TX to RX.

Illuminated by the TX, the RIS forms a reflected beam towards RX, by applying distinct phase-shifts on each of its unit-cells and making sure that all propagation paths coming from all unit-cells combine constructively together. In addition, the RIS applies an additional phase-offset that is common to all unit-cells. The RIS makes sure that all propagation paths coming from all unit-cells combine constructively together, with **a controlled common phase** at RX. The RIS can therefore control this phase so that:

- The RIS-to-RX path and the metallic-plate-to RX path combine **constructively**, to obtain a **boosted** received signal at RX **S_boosted**, as illustrated in Figure 8-1 e);
- The RIS-to-RX path and the metallic-plate-to RX path combine **destructively**, to **reduced or null** received signal at RX **S_nulled**, as illustrated in Figure 8-1 f).

Results reported in [RBs+23], show **20 dB** of difference between **S_boosted** and **S_nulled**.

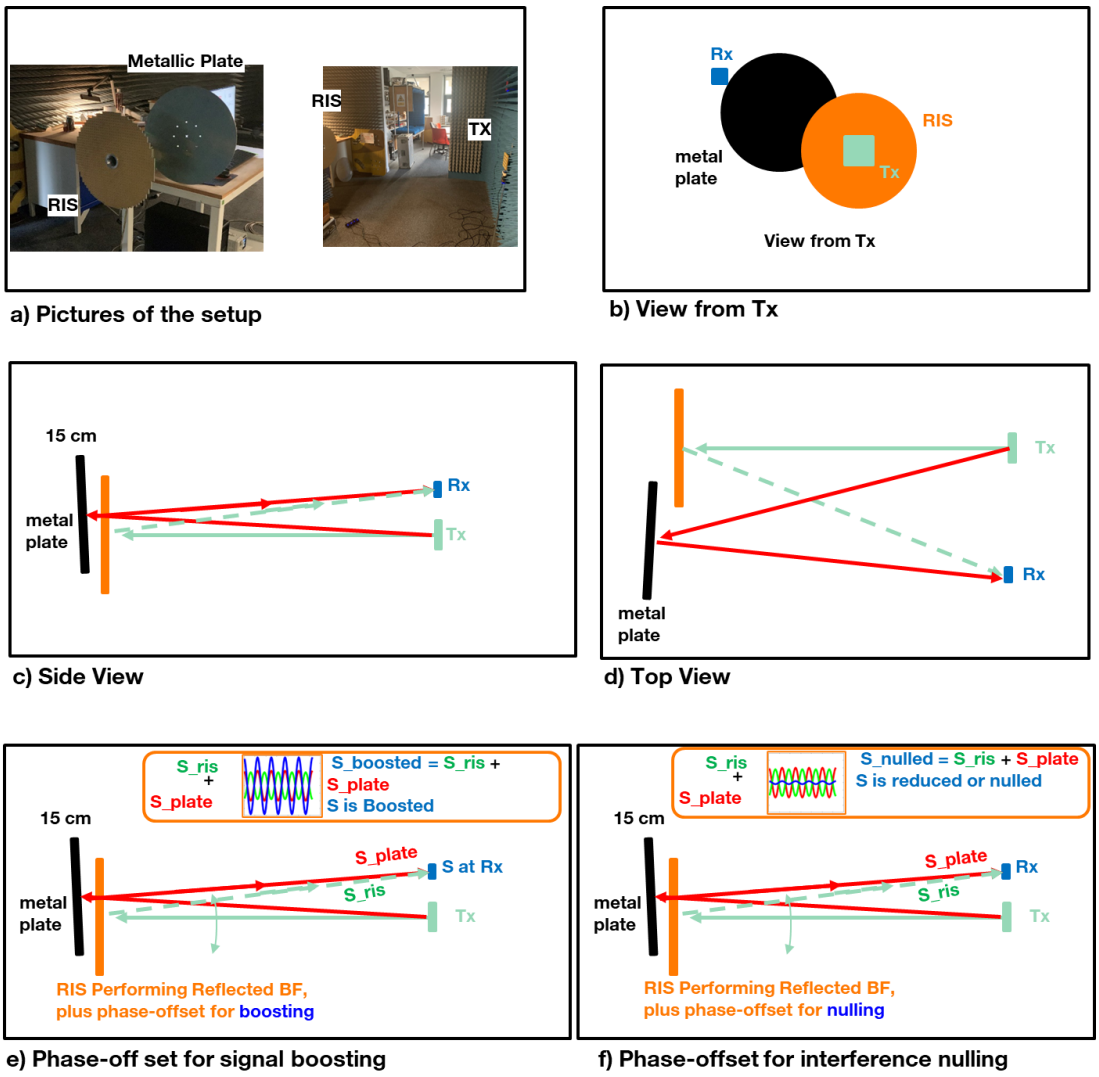

Figure 8-1 Experimental Setup.